Ocean Modelling 112 (2017) 139–153

Contents lists available at ScienceDirect

Ocean Modelling

journal homepage: www.elsevier.com/locate/ocemod

A box model for representing estuarine physical processes in Earth system models

Qiang Sun[a,*], Michael M. Whitney[a], Frank O. Bryan[b], Yu-heng Tseng[b]

[a] Department of Marine Sciences, University of Connecticut, Groton, CT 06340, USA
[b] Climate and Global Dynamics Laboratory, National Center for Atmospheric Research, P.O. Box 3000, Boulder, CO 80305, USA

ARTICLE INFO

Article history:
Received 14 July 2016
Revised 26 February 2017
Accepted 5 March 2017
Available online 6 March 2017

Keywords:
Climate modelling
Riverine freshwater
Estuarine processes

ABSTRACT

Appropriately treating riverine freshwater discharge into the oceans in Earth system models is a challenging problem. Commonly, the river runoff is discharged into the ocean models with zero salinity and arbitrarily distributed either horizontally or vertically over several grid cells. Those approaches entirely neglect estuarine physical processes that modify river inputs before they reach the open ocean. In order to realistically represent riverine freshwater inputs in Earth system models, a physically based Estuary Box Model (EBM) is developed to parameterize the mixing processes in estuaries. The EBM represents the estuary exchange circulation with a two-layer box structure. It takes as input the river volume flux from the land surface model and the subsurface salinity at the estuary mouth from the ocean model. It delivers the estuarine outflow salinity and net volume flux into and out of the estuary to the ocean model. An offline test of the EBM forced with observed conditions for the Columbia River system shows good agreement with observations of outflow salinity and high-resolution simulations of the exchange flow volume flux. To illustrate the practicality of use of the EBM in an Earth system model, the EBM is implemented for all coastal grid cells with river runoff in the Community Earth System Model (CESM). Compared to the standard version of CESM, which treats runoff as an augmentation to precipitation, the EBM increases sea surface salinity and reduces stratification near river mouths. The EBM also leads to significant regional and remote changes in CESM ocean surface salinities.

1. Introduction

Rivers deliver an annual average of 1.25 Sv (1 Sv = 1×10^6 $m^3 s^{-1}$) of freshwater to the ocean (Durack, 2015). These inputs, however, have much larger impacts on oceanic dynamics than would be guessed based on their volume flux alone. Riverine freshwater lowers surface salinity and introduces stratification that can reduce mixed layer thickness, modify currents, and influence air-sea interaction. Coles et. al. (2013) show that the Amazon River freshwater has pathways into the western tropical and subtropical gyres of the North Atlantic. In the Bay of Bengal, the summer monsoon induced riverine discharge can inhibit the air-sea heat exchange by decreasing the Sea Surface Salinity (SSS) to build a barrier layer (Vinayachandran et al., 2002). Such impacts on ocean salinities and stratification depend on how riverine freshwater initially enters the ocean (Hordoir et al., 2008). In nature, estuaries transform river inputs before they enter the ocean. Tides and other processes (e.g. winds) generate shear-driven mixing and internal wave breaking entrains saltwater into the fresher layer (Dyer, 1998). This mixing and entrainment drives an estuarine exchange flow (or gravitational circulation) that draws saltwater into estuaries; the saltwater ultimately exits along with riverine freshwater as a mixed (non-zero salinity) outflow to the coastal ocean (e.g. MacCready and Geyer, 2010). Estuaries and their mixing processes have spatial scales below that which can be explicitly represented in Earth system models (ESMs) with horizontal resolutions typically 100 km or coarser. This study develops and applies an Estuary Box Model (EBM) to represent estuarine processes in ESMs. It provides a physically-based method for introducing riverine freshwater to the model ocean without significantly increasing computational time.

2. Background

In ESMs the riverine discharge is usually introduced into the ocean component with zero salinity; implicitly neglecting any estuary mixing or exchange. In addition, instead of applying the freshwater inflow as a horizontal flux entering through the coastal boundary, the riverine freshwater is often applied to the ocean surface as a vertical flux of “augmented precipitation” over a

* Corresponding author.
E-mail address: qiang.sun@uconn.edu (Q. Sun).

http://dx.doi.org/10.1016/j.ocemod.2017.03.004
1463-5003/

specified ocean region (often hundreds of kilometers wide) surrounding the actual river mouth (Griffies et al., 2005 and Tseng et al., 2016). Some models such as the Community Earth System Model (CESM) employ the virtual salt flux (VSF) formulation that handles river inputs (and precipitation) by removing salt from the ocean surface instead of adding freshwater volume. The VSF for rivers is calculated by multiplying the freshwater volume flux with a reference salinity that is usually taken as a global constant (e.g. 34.7 PSU in the CESM) in order to assure global salt conservation. Yin et al. (2010), and Tseng et al. (2016) show the limitations of the global reference salinity and use a local reference salinity instead. These studies also distribute the riverine freshwater vertically over several layers or enhance horizontal mixing at river mouths to diffuse the freshwater horizontally. The Tseng et al. (2016) sensitivity study shows that ocean model results strongly depend on the river input methods and finds that CESM can be run successfully without the large spreading regions typically used. All these methods omit the important natural physical processes that fresh riverine runoff will be pre-mixed with saltier oceanic water within estuaries, rather than discharged into ocean with zero salinity.

Garvine and Whitney (2006) made a first attempt to parameterize the estuarine mixing processes for climate models. They built an estuary box model based on the potential energy anomaly concept introduced by Simpson et al. (1990) and compared results to observations for the Delaware Bay. Rice et al. (2008) added a two-layer formulation to this box model. Hordoir et. al. (2008) implemented a shelf box model based on the idea of potential energy anomaly (in NEMO, Nucleus for European Modelling of the Ocean) that reproduced the coastal overturning on the Mekong shelf for both upwelling- and downwelling-favorable winds. Herzfeld (2015) developed a numerical method to introduce the riverine freshwater input and include upper and lower layer exchange by considering estuary salt wedge adjustment that is most appropriate for highly stratified estuaries with weak tides and/or strong river discharge. MacCready and Geyer (2010) summarize up-to-date estuarine mixing parameterizations in their review paper. Their review provides the theoretical basis and parameterizations that support the development of the new EBM that represents the essential influence of estuarine exchange flow. In this study we focus on the formulation of a new EBM and its calibration and validation against observations for a well-observed estuary system – the Columbia River. We additionally demonstrate the practicality of its application in ESMs, and make an initial assessment of its impact in a global simulation with the CESM. A more thorough analysis of impacts on the global climate, the sensitivity to parameter choices within the EBM, and broader comparisons with observations will be addressed in subsequent studies.

3. Estuary box model development

3.1. Configuration

The EBM is a two-layer rectangular box with constant width (W), constant total depth (H), and time-varying length (L) (Fig. 1). Each layer has a constant thickness (h and H-h for the lower and upper layers, respectively) and a vertically uniform (but horizontally varying) salinity and density; thus, the estuary model water column is vertically piecewise constant. The salinity and density are allowed to vary horizontally to better represent horizontal gradients in salinities at the mouth boundary; the domain including the EBM and connecting ocean model has a horizontally piecewise continuous salinity solution. L is the landward extent of the lower-layer saltwater intrusion that adjusts to forcing conditions; this estuary length adjustment allows for simplifications later and better represents estuarine dynamics (MacCready and Geyer, 2010). The *x*-axis originates at the mouth and is positive towards the ocean.

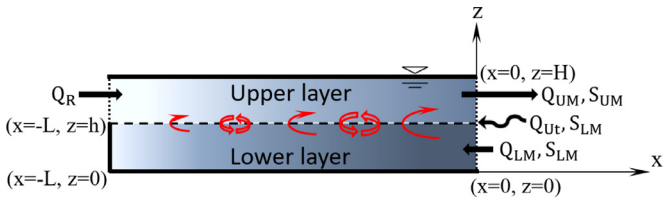

Fig. 1. Schematic representation of the EBM. Thick solid lines indicate closed boundaries, dotted lines show open boundaries, and the dashed line is the layer interface. Volume fluxes along with salinities are represented with arrows at open boundaries. Shear induced turbulent mixing (coupled upward and downward open arrows) and the upward advection associated with exchange flow (upward solid arrows) connect the upper and lower layers. The color gradient represents salinity variations from fresher (lighter shades) to saltier (darker shades) waters.

The *z*-axis is defined positive upward from the bottom. Riverine freshwater discharge (Q_R) enters through the estuary head. Oceanic saltwater flows into the EBM through the mouth lower layer (Q_{LM}); note that Q_{LM} is negative. Tidal pumping (e.g. MacCready, 2007) can drive a net horizontal salt flux into the mouth upper layer. The tidal pumping results from differences in salt advection during flood and ebb, which can be modeled as a diffusive flux in subtidal analysis (averaged over tidal variations). The upper and lower layers in the EBM communicate via vertical tidal mixing and by the upward advection (associated with estuary exchange flow). Mixed estuarine water flows to the coastal ocean though the mouth upper layer (Q_{UM}).

3.2. Continuous governing equations

The fundamental governing equations are tidally-averaged (subtidal), laterally-averaged, and steady-state. Estuaries experience non-steady-state dynamics over several time scales, but the steady-state dynamics assumed here are expected to provide a reasonable representation of the estuaries over monthly time scales. The volume balance, i.e. the incompressible continuity (Eq. (1)), involves the along-estuary and vertical velocities (u and w).

$$\frac{\partial u}{\partial x} + \frac{\partial w}{\partial z} = 0 \tag{1}$$

The salinity balance (Eq. (2)) includes advection and diffusion with horizontal and vertical eddy diffusivities (K_H and K_V).

$$\frac{\partial (uS)}{\partial x} + \frac{\partial (wS)}{\partial z} = \frac{\partial}{\partial x}\left(K_H \frac{\partial S}{\partial x}\right) + \frac{\partial}{\partial z}\left(K_V \frac{\partial S}{\partial z}\right) \tag{2}$$

A linear equation of state (Eq. (3)) is used to calculate density from salinity, where ρ_0 is 1000 kg m^{-3} and β is 7.7×10^{-4} PSU^{-1} (MacCready, 1999).

$$\rho = \rho_0 (1 + \beta S) \tag{3}$$

Converting the salinity balance (Eq. (2)) into density balance and multiplying it by gz yield the potential energy equation (Eq. (4)), where the gravitational potential energy density (PE) is ρgz.

$$\frac{\partial (uPE)}{\partial x} + \frac{\partial (wPE)}{\partial z} = \frac{\partial}{\partial x}\left[K_H \frac{\partial (PE)}{\partial x}\right] + \frac{\partial}{\partial z}\left[K_V \frac{\partial (PE)}{\partial z}\right] - K_v g \frac{\partial \rho}{\partial z} - g \frac{\partial K_v \rho}{\partial z} + wg\rho \tag{4}$$

The vertical boundary conditions are no-normal-flow through the surface and flat bottom ($w = 0$) and no density sinks or sources ($d\rho/dz = 0$). Freshwater fluxes from precipitation and evaporation are neglected within the estuary as small relative to the river inputs. In the following sections, the continuous governing equations are integrated over the estuary domain and parameterizations are applied where required.

3.3. Estuary-integrated volume and density balances

Vertically and horizontally integrating the continuous volume balance (Eq. (1)) over the entire estuary box domain yields an estuary integrated balance between the river inflow, lower-layer inflow, and upper-layer outflow at the mouth (Eq. (5)); Q_{UM} and Q_R are positive and Q_{LM} is negative.

$$\mathbf{Q_{UM}} + \mathbf{Q_{LM}} - \mathbf{Q_R} = 0 \tag{5}$$

After vertically integrating the continuous salinity equation (Eq. (2)) the vertical advection and vertical diffusion terms become zero (because of vertical boundary conditions). Subsequent horizontal integration (of the equivalent density equation) yields an estuary-integrated balance (Eq. (6)) among mass fluxes associated with subtidal flow and horizontal diffusion through the mouth upper-layer (associated with tidal pumping), and it is assumed there is no diffusion through the other boundaries.

$$\rho_{LM}Q_{LM} + \rho_{UM}Q_{UM} - \rho_R Q_R = (\rho_{LM} - \rho_{UM})a_0 a_t \frac{Q_{Ut}}{2} \tag{6}$$

The tidal pumping term is based on Stommel and Farmer (1952) and MacCready (2007) and derived in the Appendix. Q_{Ut} is defined as positive and is the average tidal volume flux during half a tidal cycle, with $Q_{Ut} = 2W(H-h)u_t/\pi$ (as in Eq. A2)) where u_t is the tidal current amplitude. The geometric coefficient a_t (Eqs. (A10) and (A11)) represents the fraction of tidal volume exchange in which the saltier oceanic water replaces estuarine water. MacCready (2007) found that the horizontal diffusion at the estuarine mouth might be overestimated by using this approach, so a coefficient a_0 is included as a free parameter. Note that ρ_{LM} (S_{LM}) is used to represent the density (salinity) entering from outside the estuary. Also note that ρ_{UM} represents upper-layer conditions at the estuary mouth open boundary and is greater than or equal to the upper layer-averaged density within the estuary.

3.4. Estuary-integrated potential energy balance

Vertically and horizontally integrating the continuous PE equation (Eq. (4)) and multiplying by the estuary width yields the estuary-integrated PE balance (Eq. (7)).

$$\begin{aligned}&\frac{1}{2}g\rho_{LM}Q_{LM}h + \frac{1}{2}g(\rho_{UM}Q_{UM} - \rho_R Q_R)(H+h)\\ &= \frac{1}{4}a_0 a_t g(\rho_{LM} - \rho_{UM})Q_{Ut}(H+h) + K_V g W\int_{-L}^{0}[\rho_L(x) - \rho_U(x)]dx\\ &\quad + W\int_{-L}^{0}\int_{0}^{H} wg\rho dz dx\end{aligned} \tag{7}$$

The terms on the left-hand side represent advection of PE due to horizontal fluxes into or out of the estuary. The first term on the right-hand side of Eq. (7) is upper-layer integrated horizontal diffusion at the mouth (tidal pumping), which is parameterized as in the density balance (Eq. (6)). The next term is from the vertical diffusion of PE and has been written assuming K_V is vertically uniform. The estuary-integrated vertical diffusion terms are non-zero because of the z dependence in the second, third and fourth terms on the right-hand side of the continuous PE equation (Eq. (4)). The vertical diffusion increases the potential energy in the water column, so it has the positive sign. The integrals for the mass lifting term, the final term in Eq. (7), are evaluated in next section.

3.5. Vertical velocity, density distribution, and estuary length

It is assumed that the vertical velocity w in the estuary box is independent of x. The w vertical profile is approximated by a vertically piecewise linear function (Eq. (8)) with a maximal positive (upward) value w_i at the layer interface and zeros at the surface and bottom.

$$w(z) = \begin{cases} w_i\dfrac{H-z}{H-h} & h < z \le H \\ w_i\dfrac{z}{h} & 0 \le z \le h \end{cases} \tag{8}$$

Because of the steady-state volume balance, vertical volume flux exiting the lower layer through the layer interface ($w_i LW$) must equal $-Q_{LM}$. By substituting $w_i = -Q_{LM}/(LW)$ and integrating $wg\rho$ over the EBM, the (positive) lifting term in the PE balance (**Eq. (7)**) is solved in Eq. (9).

$$\int_{-L}^{0}\int_{0}^{H} wg\rho dz dx = -\frac{1}{2}g\frac{Q_{LM}}{LW}\left[(H-h)\int_{-L}^{0}\rho_U(x)dx + h\int_{-L}^{0}\rho_L(x)dx\right] \tag{9}$$

A linear density distribution (in the x-direction) with a constant layer density difference is employed in the exchange-dominated solution of MacCready (1999) and other studies (e.g. Huijts et al., 2009). Observations also suggest the linear approximation is appropriate (Garvine et al., 1992). Consequently, the horizontal density distribution is approximated by linear functions in each EBM layer (Eq. (10)).

$$\rho_U(x) = \begin{cases} \frac{\rho_{LM}-\rho_R}{L}x + \rho_{UM} & -\Delta x < x \le 0 \\ \rho_R & -L \le x \le -\Delta x \end{cases} \text{with } \Delta x = \frac{\rho_{UM}-\rho_R}{\rho_{LM}-\rho_R}L$$
$$\rho_L(x) = \frac{\rho_{LM}-\rho_R}{L}x + \rho_{LM} - L \le x \le 0 \tag{10}$$

The density distribution is horizontally piecewise continuous with ocean-side salinities at the mouth; there the upper and lower layer densities reach ρ_{UM} and ρ_{LM}, respectively. The layer density difference is constant except in the segment from Δx (where the upper-layer starts to deviate from 0 PSU and ρ_R) to the head of EBM (where the lower-layer reaches 0 PSU and ρ_R) where layer density difference linearly decreases to zero. From these approximations, the density integrals in (Eq. (7) and Eq. (9)) can be solved analytically (Eq. (11)).

$$\begin{aligned}\int_{-L}^{0}\rho_U(x)dx &= \frac{1}{2}\frac{\rho_{UM}^2 - \rho_R^2}{\rho_{LM}-\rho_R}L + \frac{(\rho_{LM}-\rho_{UM})\rho_R}{\rho_{LM}-\rho_R}L\\ \int_{-L}^{0}\rho_L(x)dx &= \frac{1}{2}(\rho_{LM}+\rho_R)L\end{aligned} \tag{11}$$

MacCready and Geyer (2010) provide the length scale (L) of the estuary salinity intrusion in exchange-dominated estuaries (Eq. (12)).

$$L = 0.024a_1\left(\frac{WHc^4}{Q_R Sc^2}\right)^{1/3}\frac{H^2}{K_V} \text{ with } c = \sqrt{g\beta S_{LM}H} \tag{12}$$

In this equation, a_1 is an adjustment coefficient, c is an upper bound for the internal wave speed, and Sc is Schmidt Number (Sc = 2.2 for this application). The Schmidt Number may vary from estuary to estuary in nature, but the value chosen here is commonly used for estuarine studies. The underlying principle is the salinity intrusion has adjusted to river discharge and mixing conditions (represented by K_V). Applying this fully-adjusted length scale is consistent with the EBM steady-state dynamics and ultimately removes the K_V dependence in the solution (as derived below). Therefore, it reduces the number of parameters required by the EBM.

Eqs. (8)–(12) are substituted into Eq. (7) to yield a new form of the PE balance (Eq. (13)).

$$\begin{aligned}&\frac{1}{2}g\rho_{LM}Q_{LM}h + \frac{1}{2}g(\rho_{UM}Q_{UM} - \rho_R Q_R)(H+h)\\ &= \frac{1}{4}a_0 a_t g(\rho_{LM} - \rho_{UM})Q_{Ut}(H+h)\end{aligned}$$

$$+0.012a_1\left(\frac{WHc^4}{Q_R Sc^2}\right)^{1/3} g(\rho_{LM}-\rho_{UM})\frac{(\rho_{LM}+\rho_{UM}-2\rho_R)}{\rho_{LM}-\rho_R}WH^2$$
$$-\frac{1}{4}g\frac{(H-h)\left(\rho_{UM}^2+2\rho_{LM}\rho_R-2\rho_{UM}\rho_R\right)-H\rho_R^2+h\rho_{LM}^2}{\rho_{LM}-\rho_R}Q_{LM} \quad (13)$$

The PE balance depends on fluxes and densities at the mouth and head, estuary width, layer thicknesses and total depth, the geometric coefficient for tidal pumping (a_t is set in Eq. (A10) or Eq. (A11)) and two free parameters (a_0 and a_1) that can be used to tune horizontal diffusion and vertical mixing strength for a given estuary. The left-hand side of the Eq. (13) represents the PE fluxes directly associated with horizontal advection through the head and mouth, while the right-hand side includes the contributions of tidal pumping through the mouth, estuarine mixing, and upwelling associated with estuary exchange flow.

3.6. Dimensional solution

The steady-state volume, density, and potential energy layer integrated balances (Eqs. 5,6, and 13) constitute a system of nonlinear equations to solve the three unknowns Q_{LM}, Q_{UM}, and ρ_{UM}. S_{UM} is found afterwards by applying the linear equation of state (Eq. (3)). Substituting Eq. (5) and(6) into equation Eq. (13) gives a cubic polynomial function (Eq. (14)) that yields Q_{LM}.

$$\lambda_3 Q_{LM}^3+\lambda_2 Q_{LM}^2+\lambda_1 Q_{LM}+\lambda_0=0 \text{ with}$$
$$\lambda_3=-H$$
$$\lambda_2=2Q_R(2H-h)+a_0a_tQ_{Ut}H$$
$$\lambda_1=0.096a_1\left(\frac{WHc^4}{Q_R Sc^2}\right)^{1/3}H^2WQ_R-Q_R(2H-h)(Q_R+a_0a_tQ_{Ut})$$
$$-a_0^2a_t^2\frac{Q_{Ut}^2}{4}H$$
$$\lambda_0=-0.048a_1\left(\frac{WHc^4}{Q_R Sc^2}\right)^{1/3}H^2W(Q_R+a_0a_tQ_{Ut})Q_R \quad (14)$$

For the EBM, only the negative real root of the Q_{LM} makes sense physically (indicating lower-layer flow into the estuary) and Eq. (14) always has only one valid root with positive a_0 and a_1 values. Substituting the Q_{LM} solution into volume conservation (Eq. (5)) yields the Q_{UM} solution in Eq. (15).

$$Q_{UM}=Q_R-Q_{LM} \quad (15)$$

Subsequently, ρ_{UM} is gained from water mass conservation (Eq. (6)) as given in Eq. (16).

$$\rho_{UM}=\left(\rho_R Q_R-\rho_{LM}Q_{LM}+\rho_{LM}a_0a_t\frac{Q_{Ut}}{2}\right)\Big/\left(Q_{UM}+\frac{a_0a_tQ_{Ut}}{2}\right) \quad (16)$$

S_{UM} can be solved using the linear equation of state (Eq. (3)) with ρ_{UM} calculated in Eq. (16). Alternately, substituting the linear equation of state (Eq. (3)) for all the densities in Eq. (16) and applying the volume balance (Eq. (5)) yields an equation for S_{UM} that is analogous to Eq. (16) but with the densities replaced by salinities (Eq. (17)).

$$S_{UM}=S_{LM}\left(-Q_{LM}+\frac{a_0a_tQ_{Ut}}{2}\right)\Big/\left(Q_{UM}+\frac{a_0a_tQ_{Ut}}{2}\right) \quad (17)$$

Note that S_{UM} reduces to $S_{LM}|Q_{LM}|/Q_{UM}$ if tidal pumping is omitted by setting a_0 to zero.

3.7. Implementation of EBM in Earth system models

3.7.1. Implementation as lateral boundary condition

The EBM can be implemented in global ocean models in a straightforward manner by specifying horizontal volume and salt fluxes through the land-ocean coastal boundary. This coupling approach is a modification to that used by Herzfeld (2015) in a regional model and Griffies et al (2005) in a global model. The specified upper layer (H_U) in the global ocean model is where the volume and salt fluxes enter the ocean, and the lower layer (H_L) is where volume and salt fluxes are removed from ocean (Fig. 2a). Note that the coupling layer thicknesses H_U and H_L do not have to match the EBM layer thickness (H-h) and h and often will be thicker due to the coarser vertical resolution in many global ocean models. Coupling the EBM maintains zero net salt flux over the water column at the coastal boundary because the salt removed from ocean model lower levels is returned (and effectively upwelled) to the upper levels. The EBM exchange flow also does not create net volume flux through the coastal boundary and the net volume flux is entirely associated with the river runoff.

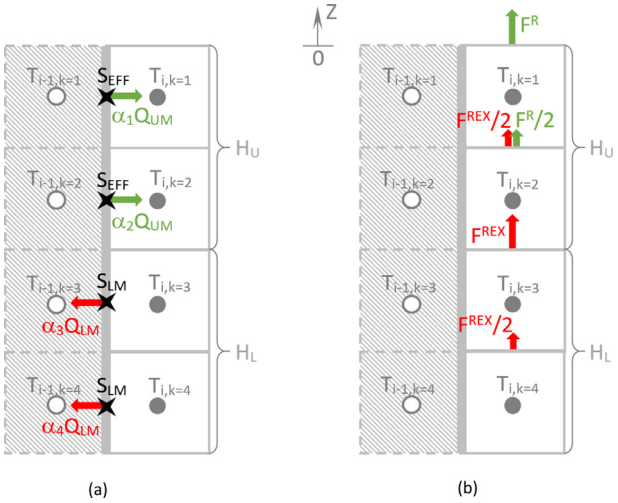

Fig. 2. Schematic representation of EBM implementations for the climate ocean models with a) real boundary fluxes treatment and b) virtual salt fluxes treatment. The solid or dashed lines bounded boxes are the typical numerical grid cells with tracer point "T" in the middle. The shaded grid cells are on land and the thicker solid lines show the vertical ocean-land boundaries. The colored arrows indicate the volume fluxes in (a) and virtual salt fluxes in (b) cross the grid faces, and the 4-points stars are located where the salinity values given by EBM. The H_U and H_L show the upper and lower layer thicknesses in POP2. The values of VSF (F^R and F^{REX}) on the grid cell interfaces shown in the (b) are practically for the POP2 with equal dZ_k.

The volume fluxes through the specified upper and lower layer at the ocean model coastal boundary can be implemented following Eq. (18).

$$Q(Z)=\begin{cases}\alpha(Z)Q_{UM} & -H_U<Z\le 0\\ \alpha(Z)Q_{LM} & -(H_U+H_L)<Z\le -H_U\\ 0 & Z\le -(H_U+H_L)\end{cases}$$
$$\text{with}\begin{cases}\sum_{-H_U}^{0}\alpha(Z)=1\\ \sum_{-(H_U+H_L)}^{-H_U}\alpha(Z)=1\end{cases} \quad (18)$$

The model vertical coordinate Z in Eq. (18) is positive upwards from the surface, Z is negative throughout the water column. The $\alpha(Z)$ is a flexible vertical weighting function, and the summation of the $\alpha(Z)$ within the upper layer has to equal one, and it is the same for the lower layer (e.g. $\alpha_1=\alpha_2=\alpha_3=\alpha_4=0.5$ in the Fig. 2a). The volume flux Q_{UM} is positive since it enters the ocean, and Q_{LM} is negative since it leaves the ocean. In practice the volume fluxes are implemented as velocities at the velocity-grid on the land-ocean interface. The approaches will vary between different numerical grid structures. For the staggered C-grid, the velocity points are

in the middle of the tracer grid cell lateral faces. Thus, the implemented velocity for each grid cell can be found by dividing the weighted volume flux by the area of the grid cell face on the land-ocean boundary. For the staggered B-grid, the velocity points are at the corners of tracer grid cell. Then the volume fluxes can be evenly split into the two adjacent velocity points. The vertical integral of volume flux will equal the riverine discharge Q_R on the ocean-land boundary after correct coupling implementation.

The lower layer salinity S_{LM} for the salt flux calculations is calculated with Eq. (19).

$$S_{LM} = \frac{\sum_{-(H_U+H_L)}^{-H_U} \left(S_{i,k} \cdot dZ_k\right)}{H_L} \tag{19}$$

The dZ_k in Eq. (19) is the thickness of the tracer grid cell at vertical level k (e.g. $dZ_3 = dZ_4$ and $S_{LM} = S_{i,3}/2 + S_{i,4}/2$ in the Fig. 2a). S_{LM} also is used to force the EBM. Salt fluxes for the upper layer involve the effective salinity S_{EFF} calculated in Eq. (20).

$$S_{EFF} = S_{LM} \frac{Q_{LM}}{Q_{LM} - Q_R} \tag{20}$$

S_{EFF} is appropriate for the advective salinity balance $S_{EFF}Q_{UM} = S_{LM}|Q_{LM}|$ imposed by this coupling method at the coastal boundary. S_{EFF} equals S_{UM} if tidal pumping is not included in the EBM solution (i.e a_0 is zero), but is otherwise lower than S_{UM} (Eq. (17)). For all grid cells within the lower layer (H_L), the land-ocean interface should have the same tracer value S_{LM}. And for all grid cells within the upper layer (H_U), the land-ocean interface should have the same tracer value S_{EFF}. In practice, the salinity value on the ghost grid cells might need to be calculated with the employed tracer advection scheme, so that the salinity values at the land-ocean boundary can be ensured. The salt fluxes are calculated by multiplying the salinity by volume fluxes crossing the coastal boundary. The vertical integral of the total salt flux on the coastal boundary will be zero after correct coupling implementation.

3.7.2. Implementation as virtual salt fluxes

In this study, the EBM is implemented within CESM to test the global performance. The Parallel Ocean Program version 2 (POP2) is the ocean component of CESM (Danabasoglu et al., 2012). The riverine freshwater runoff in the POP2 is treated as a virtual salt flux (VSF) through the air-sea interface, so there are no volume or mass fluxes crossing the land-ocean coastal boundary. In this situation, the riverine runoff and estuarine exchange are handled as vertical salt flux convergence terms in the salinity conservation equation (Eq. (21)) (Tseng et al., 2016):

$$\frac{DS}{Dt} = \nabla(K\nabla S) + \frac{\partial}{\partial Z}\left[\kappa\left(\frac{\partial S}{\partial Z} - \gamma_S\right)\right] - \frac{\partial F^R}{\partial Z} - \frac{\partial F^{REX}}{\partial Z}$$
$$\text{with } \kappa \left.\frac{\partial S}{\partial Z}\right|_{Z=0} = -F_S(0) \text{ and } \kappa\,\gamma_S|_{Z=0} = 0 \tag{21}$$

where Z is the POP2 vertical coordinate (positive upwards from the surface, Fig. 2b), K is the isopycnal skew-diffusion tensor, κ is the diapycnal diffusivity and $\kappa\gamma_S$ is the KPP counter gradient flux in the boundary layer. The $F_S(0)$ includes all the freshwater VSF applied as surface boundary condition and is positive upwards (when salt is removed from the ocean), but this term excludes river runoff for the EBM implementations. The details of $F_S(0)$ treatment is discussed in Tseng et al. (2016). The last two terms on the right-hand side of Eq. (21) represent the salt flux convergences given by $-\partial F^*/\partial Z$. The riverine freshwater VSF F^R (Eq. (22)) and estuarine exchange flow VSF F^{REX} (Eq. (23)) are distributed vertically in the water column by specifying layer thicknesses H_U and H_L.

$$F^R(Z) = \begin{cases} F^R(0)\left(1 + \dfrac{Z}{H_U}\right) & -H_U < Z \le 0 \\ 0 & Z \le -H_U \end{cases} \text{ with } F^R(0) = Q_R S \tag{22}$$

$$F^{REX}(Z) = \begin{cases} F^{REX}(-H_U)\dfrac{-Z}{H_U} & -H_U < Z \le 0 \\ F^{REX}(-H_U)\dfrac{H_U + H_L + Z}{H_L} & -(H_U + H_L) < Z \le -H_U \\ 0 & Z \le -(H_U + H_L) \end{cases}$$
$$\text{with } F^{REX}(-H_U) = -Q_{LM}(S_{LM} - S_{EFF}) \tag{23}$$

The choice of H_U and H_L in POP2 are flexible and do not have to match the EBM layer thicknesses (H − h and h). The upper and lower layers in the POP2 each have to span at least one vertical level of the tracer grid cell. The treatment for the riverine freshwater (Eq. (22)) is same as the approach of Tseng et al. (2016). The riverine freshwater VSF F^R is positive and increases toward the ocean surface (Eq. (22)), thus F^R is divergent ($-\partial F^R/\partial Z < 0$) and makes negative contributions in the salinity conservation equation (Eq. (21)) within the upper layer (H_U). The vertical integral of $-\partial F^R/\partial Z$ over the entire water column yields $-F^R(0)$. In nature, lower-layer water is upwelled within the estuary and then transported back into the coastal ocean with the upper-layer outflow. The lower-layer (saltier) water entering the estuary is entrained from the continental shelf and there is horizontal divergence in the vicinity of the entrainment zone that requires a downwelling of near-surface (fresher) water if a steady-state volume balance is maintained. The net effects on the salinity field are bringing saltier water to the surface within the estuary and moving fresher water to deeper depths somewhere outside the estuary. In this coupling method both the upwelling and downwelling are applied within the same ocean tracer grid cells as the river runoff, thus there is no net volume flux due to exchange flow within the water column and only the vertical distribution of net salt fluxes needs to be represented. In POP2, the exchange flow is applied as upwelling VSF (F^{REX}) that increases from zero at bottom of lower layer ($-H_U - H_L$) toward the layer interface ($-H_U$), then decreases to the zero at ocean surface (Eq. (23)). Note that the Q_{LM} is negative because the water is taken away from the ocean (Fig. 1), so the F^{REX} is positive (upward) (Fig. 2b). F^{REX} is convergent ($-\partial F^{REX}/\partial Z > 0$, positive contributions in Eq. (21)) within the upper layer ($Z > -H_U$) and divergent ($-\partial F^{REX}/\partial Z < 0$, negative contributions in Eq. (21)) within the lower layer (Fig. 2b). The tracer values for calculating F^{REX} are the lower layer salinity S_{LM} (Eq. (19)), and the effective estuarine outflow salinity S_{EFF} (Eq. (20)). With this coupling method, the exchange volume flux balances within the same column of ocean grid cells, so the vertical integral of $-\partial F^{REX}/\partial Z$ over the water column is zero.

4. Columbia river test case

4.1. Observational data

The EBM is tested and evaluated for the Columbia River estuary with observations and output from a high-resolution Regional Ocean Modeling System (ROMS) simulation. For comparisons with observations, the EBM is forced with the daily discharge for 2013 calculated as the sum of USGS stream-gage observations on the Columbia River (#14105700) and its downstream tributaries in Willamette River (#14197900), Lewis River (#14222500 and #14220500) and Cowlitz River (#14243000). Tidal information used to assess tidal pumping is derived from the NOAA sea level record at Hammond, OR (#9439011) near the Columbia River

Table 1
Columbia EBM test case settings.

EBM Runs	Observations:Spring-neap	Observations: No spring-neap	ROMS: Spring-neap	ROMS:No spring-neap
H, h (m)	10.93, 5.47	10.93, 5.47	10.93, 5.47	10.93, 5.47
W (km)	3.67	3.67	3.67	3.67
River forcing	Daily USGS Q_R	Filtered Daily USGS Q_R	Daily ROMS Q_R	Filtered Daily ROMS Q_R
Tidal forcing	Daily NOAA u_t	$u_t = 0.96$ (m s^{-1})	Daily NOAA u_t	$u_t = 0.96$ (m s^{-1})
S_{LM} (PSU)	32	32	ROMS S_{LM}	Filtered ROMS S_{LM}
Coefficients	$a_0 = 1.2$, $a_1 = 0.93$	$a_2 = 0.7$, $a_1 = 0.93$	$a_0 = 1.2$, $a_1 = 0.93$	$a_2 = 0.7$, $a_1 = 0.93$
a0*at=a2	1.2*(varying at)=(varying a2)	1.2*0.59 = 0.7	1.2*(varying at)=(varying a2)	1.2*0.59 = 0.7
Comparison	Daily NOAA S_{UM}	Filtered NOAA S_{UM}	ROMS S_{UM}, Q_{UM}	ROMS S_{UM}, Q_{UM}

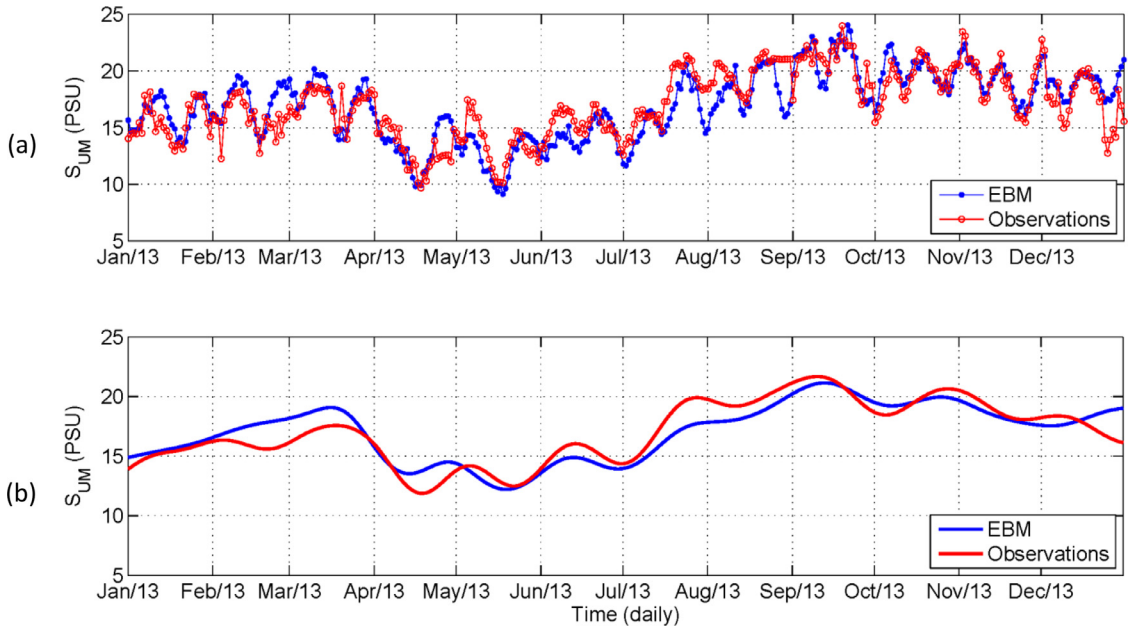

Fig. 3. Comparisons of daily mean outflow salinity given by the EBM (blue) and observations (red) for 2013 at the Columbia River mouth. (a) With the spring-neap Q_r and u_t and (b) without spring-neap tidal variations. (For interpretation of the references to color in this figure legend, the reader is referred to the web version of this article.)

mouth. The daily tidal amplitude (η_t) is set by averaging the two high tides each day if the EBM forcing includes the spring-neap tidal variations. Otherwise, the record-averaged tidal amplitude is used. The corresponding tidal velocity amplitude (u_t) forcing is estimated from the depth-averaged long-wave solution $u_t = \eta_t\sqrt{g/H}$. The EBM upper-layer salinities are compared to daily-averaged estuarine outflow salinities calculated from observations collected at the NOAA National Data Buoy Center Station JTAW1 (collected 6.4 m below mean water level at a 6 min. interval). Any data gaps are linearly interpolated prior to daily averaging. The oceanic inflow water salinity is set to 32 PSU since no observational record is available for the time period. This value is a reasonable estimate for ambient shelf waters, but it excludes time variations of shelf-water salinity. The total depth of estuary box is calculated from the General Bathymetric Chart of the Oceans (GEBCO) global 30 arc-second data, which gives the root mean squared depth of 10.93 m. The EBM upper layer has the same thickness as the lower layer (the interface is at mid-depth). The box width is set to 3.67 km, the mouth width measured from Google Earth.

4.2. Comparisons with observations

In this testing, the diffusion adjusting constants a_0 and a_1 are constrained using the MATLAB function "fminsearch" (Lagarias et al., 1998), that gives optimized parameters for the smallest Root Mean Squared Error (RMSE) of outflow salinities between EBM and observations. The best-fit values are $a_0 = 1.20$ and $a_1 = 0.93$ (Table 1). The observed Columbia River estuary outflow salinities show clear spring-neap tidal variations (Fig. 3a), with amplitudes of approximately 5 to 8 PSU. Outflow salinities are fresher between April and July and saltier from August to December due to the river discharge annual cycle. The EBM solution performs well in representing both the spring-neap outflow salinity variations and the seasonal salinity changes (Fig. 3). The RMSE between EBM results and observations is 1.7 PSU (10% of the observed mean outflow salinity) with the squared correlation coefficient (r^2) of 0.70 and bias of −0.06 PSU.

For ESMs focused on long-term variations of the global ocean, the spring-neap tidal variations may become less important. So the EBM without spring-neap tidal variations is tested with constant tidal amplitude ($\eta_t = 1.01$ m, $u_t = 0.96$ m s^{-1}). A 5th order Butterworth low-pass filter with cut-off period of 33 days is employed to filter out the spring-neap signals (and higher frequency variations) from the observed river discharge for forcing and the observed outflow salinity data for comparison. The a_1 value (0.93) is kept the same as before. In this case, the tidal pumping geometric ratio a_t is constant, so it is combined with a_0 to yield the tidal pumping adjusting constant $a_2 = a_0 a_t$. This simplifies the EBM parameter space in the ESMs. The optimization function gives $a_2 = 0.70$. The EBM calculated outflow salinities compared to the filtered observations have RMSE of 1.11 PSU, r^2 of 0.81 and mean bias of −0.02 PSU (Fig. 3b). The EBM follows the seasonal variation of Columbia River outflow salinities, although it has a saltier outflow in spring and fresher outflow in summer. The EBM works well to represent the estuary outflow salinity in the case of Columbia River, which encourages its application to other estuaries and within ESMs.

4.3. ROMS simulation data

Observational time series of volume fluxes at estuary mouths are uncommon, but regional ocean models can provide these fluxes. A pre-existing ROMS simulation of the Columbia River and the adjacent ocean region provides a comparison for EBM results. The model details are described in Giddings et al. (2014). The comparison data are the ROMS results for 2005. They are tidally averaged with a low-pass Godin 24/24/25 filter (Godin, 1972). Volume fluxes are calculated at the head (Q_R forcing for the EBM) and at the estuary mouth (Q_{UM} and Q_{LM} for comparison with EBM). Q_{LM} for ROMS is determined by the spatially integrating all landward velocities through the mouth. Q_{UM} for ROMS is calculated according to Eq. (5) for the most consistent comparison with EBM steady dynamics. The calculated Q_{UM} is somewhat lower than the spatial integral of seaward velocities through the mouth because it omits the seaward compensation flow for the landward Stokes transport (Ianniello, 1979 and 1981) that is not included in EBM dynamics. The ROMS inflow salinities through the mouth (S_{LM} forcing for EBM) are calculated by dividing total landward salinity fluxes through the mouth by Q_{LM}. The ROMS outflow salinities (S_{UM} for comparison with EBM) are calculated in analogous fashion to S_{LM} and can be compared to EBM output. EBM tidal forcing for 2005 is calculated from observed harmonic constituents as in the previous comparison. The same estuary box dimensions are employed as for the comparison with observations, and the mixing constants a_0 and a_1 also are kept same as the previous observation comparison run, so that the EBM parameter values can be evaluated with ROMS results.

4.4. Comparison to the ROMS simulation

The comparisons of EBM with ROMS are shown in Fig. 4. For the estuarine outflow salinity (Fig. 4a), EBM has a RMSE of 3.11, r^2 of 0.54 and bias of −1.33 PSU. The agreement can be increased by changing the mixing coefficients to find the best-fit EBM solution for ROMS, but this was not done as the coefficients already are set based on observations. The EBM includes the spring-neap cycles of the outflow salinity, although their amplitudes are smaller than in ROMS. In general, the lower-layer inflow salinity has much smaller variations than the upper-layer outflow salinity which has considerable variability associated with tides and river discharge. A couple of shelf freshening events in March and May cause drops of EBM outflow salinity that are not shown in the ROMS simulation. The mismatch is attributed to the EBM steady state salt balance that does not allow for a delayed and smoothed response to sudden forcing changes seen in nature (MacCready, 1999) (MacCready, 2007) and the ROMS results. This is not a major limitation in ESMs since periods of interest are usually seasonal to multi-decadal variability and estuary response generally occurs over shorter time scales.

The outflow volume fluxes from EBM matches well with ROMS results (Fig. 4b), with RMSE of 513 $m^3 s^{-1}$ (7.6% of the ROMS mean outflow volume flux), r^2 of 0.89 and a 125 $m^3 s^{-1}$ bias. The lower-layer inflow volume fluxes from the EBM and ROMS have similar mean values, but the EBM result has less high-frequency variability. In the high discharge period, the EBM tends to overestimate the outflow volume flux. Physically, with rising river discharge, the stratification in an estuary increases, which can inhibit turbulent mixing through the layer interface and reduce estuary exchange flow. In the case of Columbia River estuary, it changes from a partially mixed type to the salt wedge type with increased vertical stratification. EBM can capture the estuarine type transition by reducing the lower-layer volume flux (associated with estuary exchange flow), but it has a weaker response than in ROMS. Nevertheless, EBM works well to represent the seasonal, even spring-neap, variations of Columbia River estuary outflow volume flux from ROMS results.

To test the EBM without the spring-neap tidal signal, all ROMS data are smoothed with the same low-pass filter used for the no-spring-neap observational data. The filtered river discharge and lower-layer salinity are used to force the EBM, and the filtered outflow volume fluxes and salinities are compared to EBM results. The EBM employs the same dynamic parameters as in the comparison with the filtered observations (Table 1). The agreement is improved with RMSE of 1.74 PSU, r^2 of 0.82 and a −1.20 PSU bias for outflow salinity, and RMSE of 330 m^3/s, r^2 of 0.98 and a 123 $m^3 s^{-1}$ bias for outflow volume fluxes (Fig. 4c and d). It indicates that the EBM works well for long-period or low-frequency forcing. As the high frequency forcing is filtered out, estuaries tend to achieve a quasi-steady-state balance that is well represented by EBM steady-state dynamics. Thus, the EBM can work well in the ESMs even though it neglects the short-term estuary adjustment.

5. Applying the EBM globally

One challenge to implementing the EBM in an ESM is specifying parameters for all estuaries globally. The Dai and Trenberth (2002) dataset shows that the 20 largest rivers (the global top 20) contribute to over 60% of total global riverine freshwater runoff into the oceans. The Amazon River alone accounts for almost 25% of total global discharge. Many of the largest rivers have been well studied, therefore observational data and/or regional simulations exist to calibrate EBM mixing parameters and set box geometry. The Columbia River is a good example that has both observational and simulation data. Smaller rivers in the dataset have smaller individual contributions on freshwater discharge, but their summation is significant globally and their individual inputs are important locally. Many of these rivers do not have enough data to calibrate EBM parameters. A short path to get the EBM working for these rivers is to find a universal relationship between riverine forcing and estuarine response.

Hansen and Rattray (1966) developed the stratification-circulation diagram to quantitatively classify estuaries. They found that scaled stratification $\delta S/S_0$ (the top-to-bottom salinity difference divided by the sectional mean) in the estuary depends on the densimetric Froude number $Q_R/(cWH)$. In general, the stratification increases with rising Froude number. The EBM can be parameterized for the rivers outside of global top 20 in an ESM, so that their outflow salinities (and mouth stratification) follow this general trend. The original scaled stratification is modified to $(S_{LM}-S_{UM})/S_{LM}$ for application at the EBM mouth. Geyer (2010) applied observations from 13 estuaries (Fig. 5), and shows that the bulk stratification rises with increasing densimetric Froude number. Geyer (2010) includes two scalings to predict stratification, but they overestimate stratification for estuaries with high densimetric Froude numbers and do not asymptote to the completely stratified limit.

The EBM is set up with a uniform box frame with H= 10 m and h= 5 m. The mixing parameters of the EBM are then optimized to get the smallest RMSE for all with observation points on Fig. 5. The width scales out of the solution when expressed in terms of the densimetric Froude number; consequently, the width does not need to be specified. One EBM run includes tidal pumping with $u_t = 1$ m/s and the other neglects tidal pumping by setting a_2 to zero. The EBM solutions follow the general trend of the observations. EBM solutions with or without tidal pumping both converge and asymptote to complete stratification at high flow conditions with larger riverine densimetric Froude numbers. In the lower Froude number region, the EBM with tidal pumping has less stratification, because the tidal pumping helps to increase the estuarine outflow salinity. These results encourage the global

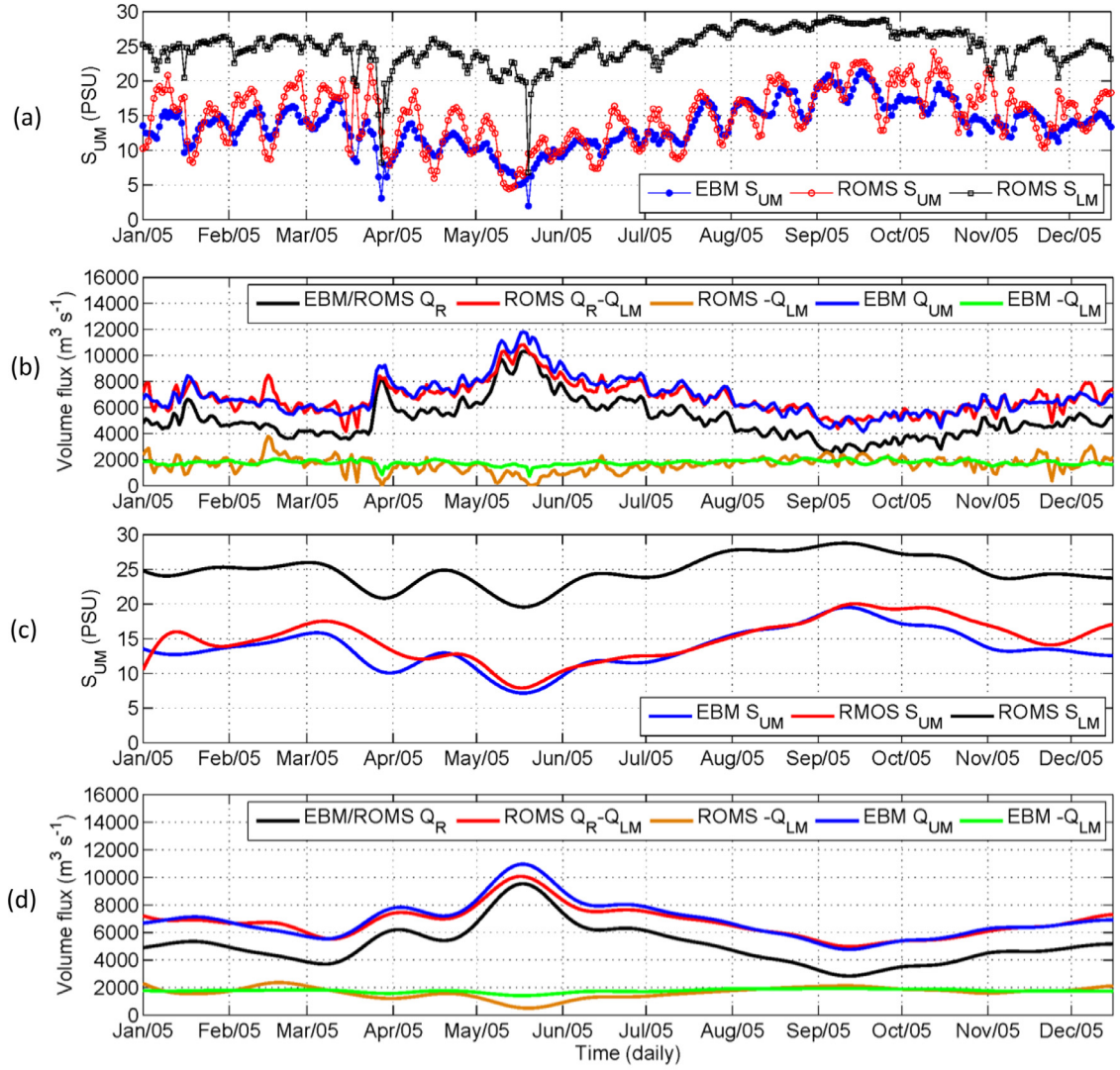

Fig. 4. Columbia River estuary comparisons between the EBM solution and the ROMS simulation. (a) and (b) compare salinity and volume fluxes with spring-neap tidal variations included. (c) and (d) compare salinity and volume fluxes without spring-neap tidal variability.

application of the EBM and indicate that even the solution without tidal pumping works well. They provide a basis for generic EBM parameters that can be applied even if there is not enough information to set estuary-specific values.

6. EBM test in global climate model

6.1. CESM and EBM settings

The EBM is implemented and tested in the ocean component POP2 of the CESM version 1.1.1 with nominal 1° horizontal resolution. POP2 has 60 vertical z-levels with 10 m resolution in the first 15 levels and is stretched to 250 m resolution for the deepest ocean. For the runs discussed here, the ocean and sea-ice components are active, while the atmospheric component and river freshwater input are decoupled and prescribed with the 1948–2007 COREII forcing (Large and Yeager, 2009; Griffies et al, 2009). The model is run for 60 years (one cycle of the forcing), and the climatological averages of the last 30 years' results are used for evaluations.

The EBM parameters are specified individually for each of the global top 20 rivers (Table 2). The total depth (H) is either picked from literature or calculated from the General Bathymetric Chart of the Oceans (GEBCO) data set (IOC, et al., 2003) as the root mean square depth in the selected estuary area. The width (W) of the box at its mouth is either from literature or measured from the Google Earth Pro v.7.1.2.2041 with its Line Ruler tool. If there is more than one channel connecting to the ocean, the box width is taken as the combined width of the channels. The lower-layer thickness is taken as half the total depth for all rivers. The mixing parameters (a_1 and a_2) of the EBM for top 20 rivers are individually optimized to match the observed outflow salinity with MATLAB function "fminsearch" (Lagarias et al., 1998) in offline integrations. The 60-year-averaged monthly discharge of each individual river is taken from the Dai and Trenberth (2002) database. The annual mean of Mean High Water (MHW) level is regenerated from the Regional and Local Tidal Solutions of the OSU Tidal Data Inversion (Egbert & Erofeeva, 2002), literature studies, or NOAA buoys. Finally, the optimized mixing parameters are found by minimizing the RMSE between the calculated annual mean outflow salinity and comparison data from published observations or regional numerical studies. The studies used to determine the mixing parameters are listed in Table 2. For other rivers, outside of the top 20, the default EBM has a common depth of 10 m and the mouth width of 2 km. The mixing parameters are from the generic fit

Table 2
EBM parameters for top 20 rivers in POP2 of CESM, where W is the width, H is the height and h_* is the layer depth ratio(h/H) for the box dimensions. The a_1 and a_2 are the dimensionless coefficients for vertical mixing and tidal pumping in the EBM.

River Name	W (m)	H (m)	h_* (-)	a_1 (-)	a_2 (-)	References to get annual mean S_{UM}
Amazon	50,000	21.8	0.5	1.00	0	Geyer (1995)
Congo	9740	8.0	0.5	1.04	2.57	Eisma and Van Bennekom (1978)
Orinoco	17,000	10.0	0.5	1.52	0	Bone et al., (2011)
Changjiang	28,870	7.4	0.5	1.59	0	Zhang et al. (2011)
Brahmaputra	11,000	14.0	0.5	0.16	0	Rao (2005)
Mississippi	4000	12.0	0.5	1.07	3.84	Georgiou and Hanegan (2013)
Yenisey	61,500	3.8	0.5	1.29	0	Burenkov and Vasil'kov (1995)
Parana	30,000	7.5	0.5	0.58	0	Fossati and Piedra-Cueva (2008)
Lena	5800	9.3	0.5	0.11	0	Cauwet and Sidorov (1996)
Mekong	15,200	6.5	0.5	1.13	0.89	Nguyen et al. (2008)
Tocantins	62,000	16.0	0.5	0.03	0	Barthem and Schwassmann (1994)
Ob	47,270	8.6	0.5	0.02	0	Burenkov and Vasil'kov (1995)
Ganges	9000	14.0	0.5	0.05	0	Rao (2005)
Irrawaddy	35,140	22.5	0.5	0.15	0	Kravtsova et al., (2009)
St. Lawrence	4680	42.9	0.5	1.03	2.57	Ingram and Ei-Sabh (1990)
Amur	20,000	14.3	0.5	0.11	0	Shevchenko et al. (2013)
Mackenzie	25,000	2.8	0.5	1.16	0.51	Emmerton et al., (2008)
Xijiang	29,000	5.2	0.5	0.28	0	Zu and Gan (2015)
Columbia	3670	10.9	0.5	1.10	1.08	NOAA buoy jtaw1
UNIFORM	2000	10.0	0.5	0.88	0	Geyer (2010)

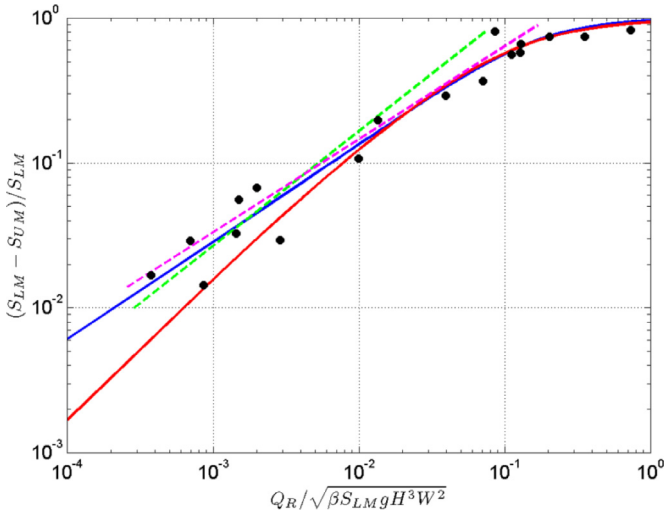

Fig. 5. Scaled stratification at estuary mouths vs. scaled river discharge (a densimetric Froude number). Black dots are observations in 13 estuaries regenerated from Geyer (2010). Dashed lines are Geyer's solutions considering tides (green) and neglecting tides (magenta). Solid (blue and red) lines are the solutions of EBM. The blue line shows the tidal pumping neglected EBM with $a_1 = 0.876$, which gives a RMSE of 0.086 and R-squared of 0.93 to the observations. And the red line with tidal amplitude of 1 m to force the tidal pumping and the mixing parameters $a_1 = 0.200$, $a_2 = 0.285$, which gives a RMSE of 0.082 and R-squared of 0.94. (For interpretation of the references to color in this figure legend, the reader is referred to the web version of this article.)

described in the previous section (Fig. 5). The contribution of tidal pumping in the default EBM is neglected.

Three test cases (VSFEBM, VSFROF, and VSFSPRD, where "VSF" indicates the virtual salt flux coupling method) are used to illustrate the effects of estuary exchange in POP2. The EBM is implemented in the VSFEBM case for all rivers in POP2. The VSFROF is a comparison case in which the EBM exchange circulation is not implemented and the same runoff ("ROF") is applied, so only riverine freshwater convergence term ($-\partial F^R/\partial Z$) is included (Eq. (21)). The layer thicknesses for coupling with CESM are $H_U = 20$ m (spanning the top two grid levels) and $H_L = 20$ m (spanning the next two grid levels) (Fig. 2b). If the local water depth is less than 40 m, H_U is held constant and H_L is reduced. Each river runoff point and the corresponding exchange flow (in VSFEBM only) is mapped to a single T-grid column near the river mouth in the VSFEBM and VSFROF cases. The VSFSPRD case represents the runoff treatment used in prior studies (e.g. Tseng et al., 2016 experiment B300CS): the riverine freshwater is included in the $F_S(0)$ term as surface boundary condition in Eq. (21) and horizontally spread over a large region (by a e-folding length scale of 1000 km with a maximum spreading radius of 300 km Gaussian distribution) rather than distributed vertically and focused horizontally at the runoff points as in the other cases. The other differences for VSFSPRD are the constant global reference salinity for riverine freshwater VSF computation (instead of a time and spatially variable reference salinity) and no EBM.

6.2. Interpretation of CESM results

The sea surface salinity (SSS) of the VSFEBM case and differences from other cases are shown in Fig. 6. Fresh regions are evident near all major river mouths. There are large differences between the VSFEBM and VSFSPRD cases that exceed 1 PSU in many areas near major rivers (the SSS difference even exceeds 7 PSU near the Amazon River mouth) (Fig. 7). VSFEBM and VSFROF are fresher than VSFSPRD adjacent to river mouths because runoff from each river is focused at one point. Introducing river inputs over large spreading regions in VSFSPRD is one reason VSFEBM and VSFROF are saltier at most other points offshore of major rivers. Also the offshore SSS is higher in VSFEBM and VSFROF because of the direct effects of vertically distributing the river inputs over a thicker layer (instead of immediately at the surface), and riverine freshwater VSF differences due to the local (instead of global) reference salinity. SSS at river mouths are further increased in VSFEBM due to the upwelling of saltier waters via estuary exchange flow VSF convergence (Eq. (21)). Indirect effects arise from coastal stratification and circulation changes as well as advection by ocean currents that transports salinity differences to remote areas (especially in the North Atlantic and Arctic) (Tseng et al., 2016).

Comparison between VSFEBM and VSFROF isolates the effects of introducing estuary exchange. VSFEBM is saltier at river runoff points because of the vertical salt flux imposed by EBM. VSFEBM is also (approximately 0.1 PSU) saltier in many coastal regions. There are, however, several regions where SSS is lower in VSFEBM; remote freshening (< 0.05 PSU) spreads into the North Atlantic that

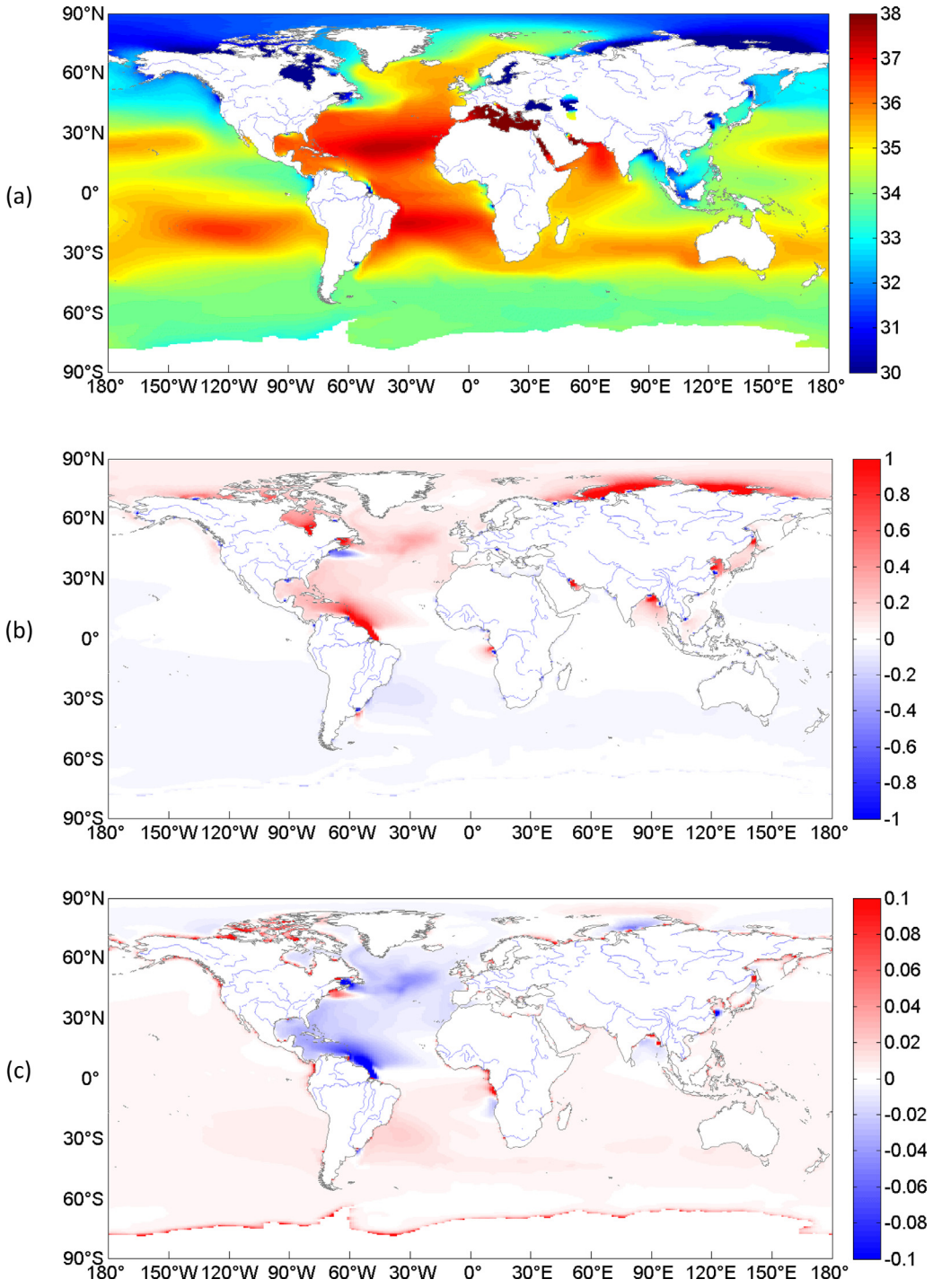

Fig. 6. (a) Sea surface salinity (SSS) of the VSFEBM case averaged over the last 30-year simulation period. The cyan lines show the global major rivers from the World Data Bank II. (b) SSS differences (VSFEBM – VSFSPRD) and (c) SSS differences (VSFEBM – VSFROF) over the same period.

is linked to the St. Lawrence and the Amazon. The freshening relative to VSFROF is counterintuitive and is linked to secondary effects resulting from modifications to stratification, ocean currents, and the local reference salinities (that evolve differently in the two cases) used in the riverine freshwater VSF calculation. Similar freshening occurs for the Changjiang, Bay of Bengal, and Kara Sea (Fig. 6). Overall, the CESM case comparison indicates significant local, regional, and even global sensitivity to including estuarine dynamics.

The Columbia and Amazon Rivers provide examples of model sensitivity to the treatment of river inputs. The SSS is freshest close to the coast near both rivers (Fig. 7). As mentioned, VSFEBM is fresher than VSFSPRD and saltier than VSFROF at the focused runoff points. For the Columbia, these same differences extend along the coast. Farther away from the coast, VSFEBM is saltier than VSFSPRD for both river regions due to the horizontal spreading of runoff in VSFSPRD and other factors mentioned above. The differences between VSFEBM and VSFROF in the Columbia show the anticipated higher SSS originating from the exchange flow VSF convergence imposed by estuary circulation. Near the Amazon, VSFEBM has lower salinities than VSFROF due to the secondary effects described above; the influence of the Amazon contributes

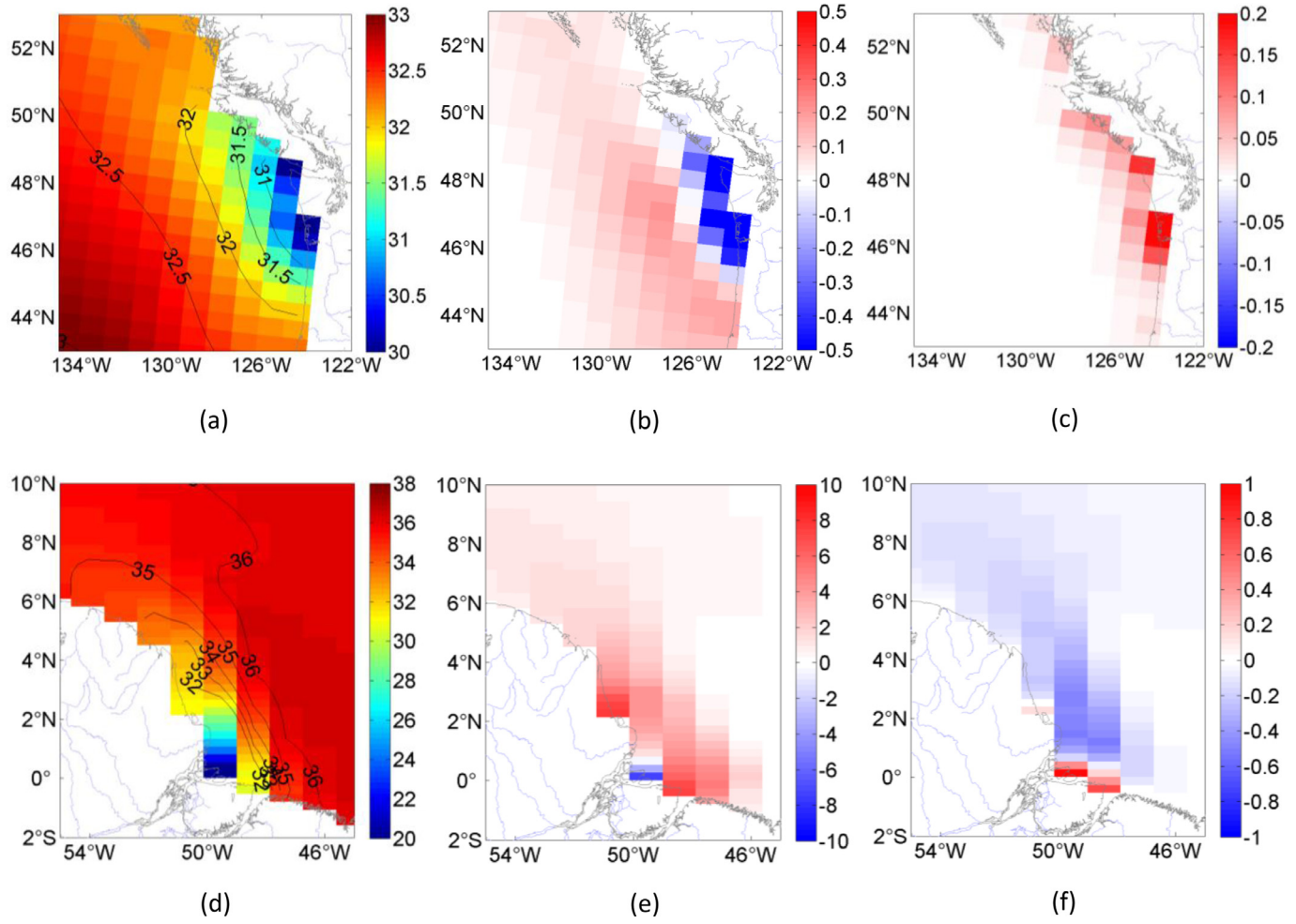

Fig. 7. SSS in the VSFEBM case around the (a) Columbia and (d) Amazon River mouths. SSS differences (VSFEBM – VSFSPRD) around the (b) Columbia and (e) Amazon River mouths. SSS differences (VSFEBM – VSFROF) around the (c) Columbia and (f) Amazon River mouths.

to differences throughout the North Atlantic. Salinity stratification near the river mouth changes among cases (Fig. 8). VSFEBM is less stratified than VSFROF and removes the problematic near-bottom salinity overshoot (> 45 PSU) near the Amazon and other large rivers that otherwise occurs for focused river inputs. The salinity overshooting is also found by Tseng et al. (2016) in the sensitivity tests of the riverine freshwater input approaches. In this previous study, the salinity over- and under-shooting occur at river mouths with large runoff and intensify as the horizontal spreading area for riverine freshwater inputs is decreased. The estuary exchange flow imposed by the EBM avoids large salinity numerical artifacts without having to impose arbitrarily large horizontal spreading regions as in VSFSPRD.

The modeled salinity profiles are further compared with salinity climatology from high resolution (0.25-degree) World Ocean Atlas 2013 (WOA) (Zweng, et al., 2013); the nearest-neighbor point to the corresponding POP grid cell are used. The spatial filtering in WOA (Zweng, et al., 2013) tends to create a positive salinity bias in the coastal ocean, especially in the regions close to the riverine freshwater sources, because typically higher offshore salinities contribute to the filtered coastal salinity values. The native World Ocean Database 2013 (WOD) salinities also are averaged within each POP T-grid cell to avoid the influence of spatial filtering. The model vertical salinity profiles at Columbia River mouth are plotted against corresponding WOA and WOD profiles (Fig. 8a). None of model results agree with climatologies through the entire water column, but VSFSPRD surface salinities are closer to the spatially filtered WOA and the other cases are closer to WOD. There are no WOD data available for the Amazon River mouth T-grid cell and the WOA has a surface salinity (at z=0) without any subsurface data; therefore no profile comparison can be made.

The sensitivity analysis in this paper has focused on long-term mean salinity fields, but seasonal cycles also are important. The seasonal SSS cycle (represented as monthly averages over the 30-year analysis period) at Columbia, Amazon, Brahmaputra and St. Lawrence river mouths are plotted for the three CESM testing runs (Fig. 9). For all four rivers, there are clear seasonal cycles that vary among the runs. The VSFSPRD case has higher salinities because the river inputs are spread over large areas (as previously described) and a seasonal cycle that can be larger (e.g. Amazon), smaller (e.g. Columbia and Brahmaputra), or similar (e.g. St. Lawrence) to the other cases. It is counterintuitive that the Amazon cycle is largest in the VSFSPRD case, but the contributing factors include no vertical spreading of the strong river runoff, changes related to the reference salinity for VSF calculation, and interactions with the ambient ocean currents. In all four rivers, the VSFEBM case has higher SSS than the VSFROF case due to the vertical salt flux imposed by estuarine exchange flows (as previously described), but the seasonal cycles are quite similar. The Brahmaputra River is discharged into the Bay of Bengal where the SSS varies strongly with monsoon seasonal wind. High-resolution ROMS results in Jana et al. (2015) show that SSS varies from lower than 24

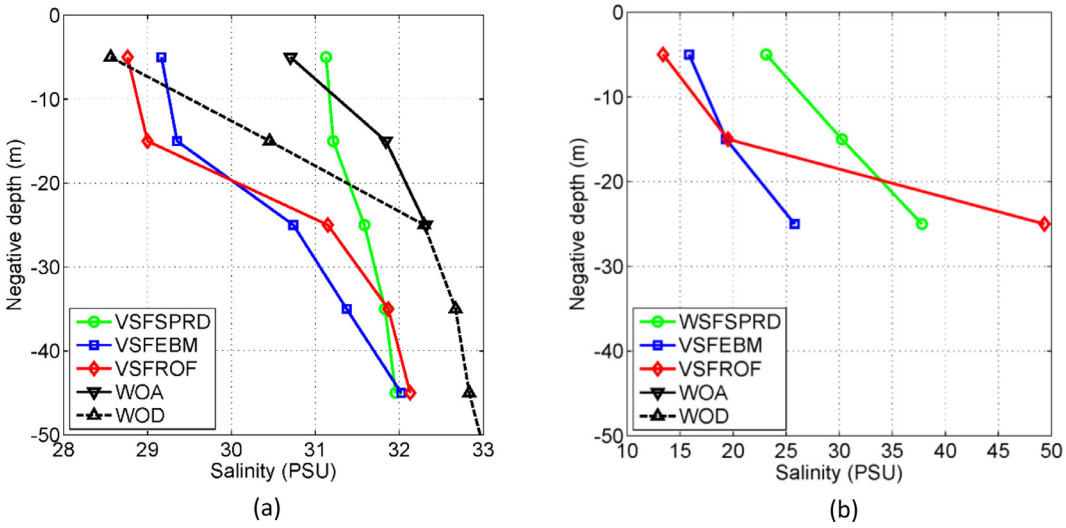

Fig. 8. Vertical salinity profiles at the (a) Columbia River mouth (123.96^o*W*, 46.76^o*N*) and (b) Amazon River mouth (49.56^o*W*, 0.13^o*N*) in POP2 for the VSFSPRD (circles), VSFEBM (squares), and VSFROF (diamonds) cases. The black triangles show the annual mean climatology data. The downward triangles are from the nearest WOA13 0.25-degree salinity to the POP2 T-grid, and the upward triangles are the POP2 T-grid cell averaged native WOD13 salinity. No WOA13 or WOD13 data are available at the Amazon mouth location.

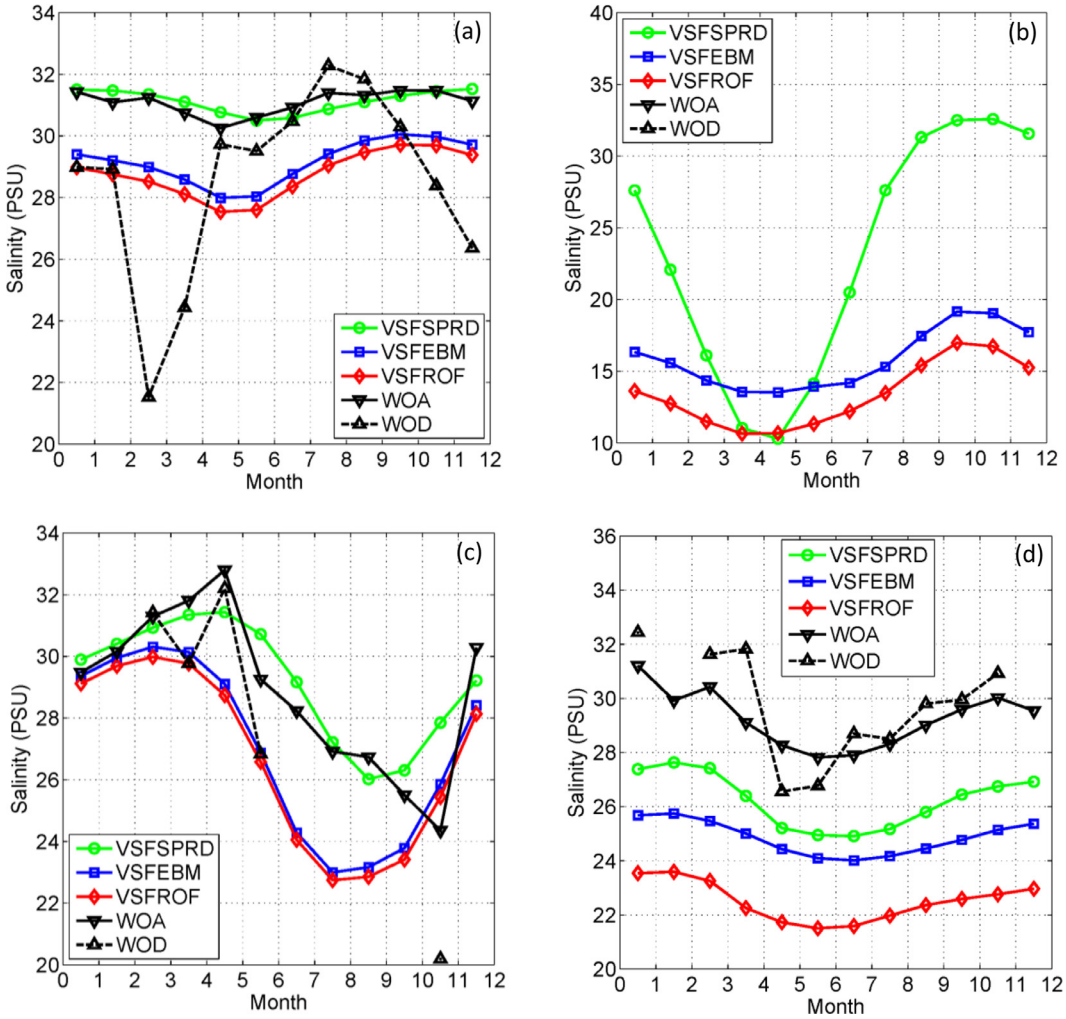

Fig. 9. 30-year averaged surface salinity seasonal cycle at (a) Columbia (123.96ºW, 46.76ºN), (b) Amazon (49.56ºW, 0.13ºN), (c) Brahmaputra (89.84ºE, 21.58ºN), and (d) St. Lawrence (67.11ºW, 49.41ºN) River mouths in POP2. The black triangles show the annual mean climatology data. Coincident WOA13 and WOD13 salinities are shown with black downward and upward triangles, respectively (as in Fig. 8).

PSU during the Indian summer monsoon season to 31 PSU during the winter monsoon period on northern Bay of Bengal. The VSFEBM SSS vary between 23 PSU and 30.2 PSU and are closest to the ROMS results for the area. The regional model of Rahaman et al. (2014) suggests the SSS varies in North Bay of Bengal between 29 to 32 PSU, while the VSFEBM results shows smaller and saltier auunal SSS change between 32 and 33 PSU.

The modeled annual SSS cycles at the four river mouths discussed above are also compared with WOA and WOD climatologies in the single T-grid cell (Fig. 9). For the Columbia, the SSS cycle for VSFSPRD is closer to WOA then other two cases, but all cases have much smaller SSS cycle amplitude than WOD (with a different timing). There are no WOD data available within the T-cell adjacent to the Amazon mouth, and the nearest WOA grid does not have subsurface salinity to make fair comparisons with POP SSS at 5 m. At the Brahmaputra River mouth, VSFSPRD is closest to WOA though the WOA amplitude is somewhat larger. The other runs are closer to the large salinity range indicated by WOD with its spiky oscillation of SSS during February to May and low salinity in October. At St. Lawrence River lower estuarine mouth, all runs are considerably fresher than the WOA and WOD salinities (VSFSPRD has the smallest different and VSFROF has the largest difference). It is worth noting that some of the SSS mismatch can be attributed to a mismatch between model runoff location and the natural riverine freshwater distribution (e.g. Saucier et al., 2003). Overall, the comparisons among model results and climatology are not conclusive. There is a tendency for VSFSPRD and WOA to be closer to each other, but this is likely because the spreading of river inputs in the model and the spatial filtering radius in WOA both smooth the sharpness of the riverine freshwater fronts near the river mouths and increase coastal salinities. VSFROF and VSFEBM have the capacity to include the lower salinities and larger annual cycles indicated by WOD, but it is hard to distinguish which run is better by these comparisons alone. It is also worth noting that differences between the WOA and WOD are at least as large as the differences among model runs. This suggests a need for an improved global climatology that pays particular attention to coastal salinities. Though the model-climatology comparisons are inconclusive, the VSFEBM configuration includes estuarine processes and therefore more of the physics governing river inputs to the ocean.

7. Discussion

Adding the estuarine exchange flows in POP2 also has impacts on the climate process beyond the costal oceans. It is shown that SSS decreases in North Atlantic and increases in the Pacific, Indian, South Atlantic, and Southern Oceans, although the change is smaller than in coastal regions (Fig. 6c). Ongoing testing (not shown here) suggests that including the EBM in the fully-coupled CESM may reduce ice formation in the Labrador Sea and can alter the Indian Ocean Dipole. In the current study, the EBM is only applied to salinity, but it will be useful to extend the approach to temperature and biogeochemical tracers in the future. Including nutrient upwelling by estuary exchange flow, for instance, likely will have significant impacts on primary productivity in global climate models in some coastal regions and perhaps farther offshore. It would be best to also include parameterizations that represent the nonconservative biogeochemical transformations within estuaries.

The EBM is designed for the specific needs of the coarse horizontal resolution climate ocean models with computational constraints. The EBM is physically-based and represents many of the essential estuarine processes. As mentioned in the introduction, Herzfeld (2015) developed a method that continuously adjusts to the landward propagation of an oceanic salt wedge into the estuary and then enforces zero net salt flux through the mouth and a net volume flux equaling river discharge. This solution does increase the salinity of the upper-layer flow from the estuary to the ocean, however it typically will have weaker exchange, be more stratified, and have a fresher upper-layer than the EBM solution since it does not include estuarine tidal mixing, a critically important factor in driving estuary exchange. It is worth mentioning that MacCready (2011) discusses an alternative approach to calculate estuarine exchange flow by using isohaline coordinates that could be incorporated into ocean models. It is important to note that high-resolution hydrodynamic models of estuaries are able to better represent individual estuaries by including more complex geometries, flow-topography interactions (e.g. sills), wind-forced circulation, and other non-steady dynamics. Consequently, coupling hydrodynamic estuarine models within ESMs will provide a more complete representation of estuarine influences on the global ocean. The computational burden, however, would be far larger than the negligble calculation times for the EBM. In future studies, it will be worthwhile to compare results for the different strategies of representing estuarine processes in ESMs.

8. Summary

The Estuary Box Model (EBM) is a physically-based approach to represent unresolved estuarine processes in global ocean models such as POP2 within the CESM. Steady-state balances for water volume, density (and salinity via the linear equation of state), and gravitational potential energy are employed. It is assumed that the estuary length (associated with the saltwater intrusion) is fully-adjusted to the river discharge and tidal mixing. Analytical solutions for estuarine outflow salinity and volume fluxes are found by considering river forcing and vertical and horizontal tidal mixing that drive estuarine exchange and transform pure river water to an outgoing mixture of freshwater and saltwater. The forcings required for the EBM are river discharge, inflowing seawater salinity, and tidal amplitude (if horizontal diffusion via tidal pumping is included). Five parameters are required for each estuary: width, total depth, lower layer thickness, and two adjustable dimensionless vertical and horizontal mixing constants.

The forcing data collected from observations and ROMS simulation are used to perform offline tests of EBM in the Columbia River estuary. The geometries of EBM box structures are calculated basic on the GEBCO and Google Earth measurements. And the mixing parameters are optimized with MATLAB intrinsic function. EBM results successfully represent seasonal outflow salinity variations associated with river discharge variability and outflow volume fluxes. The EBM is applied globally in POP2 for a CESM (sea-ice-ocean-only) run and compared to an otherwise identical case without estuary processes and a case with settings typical of prior studies. Comparisons indicate strong sensitivity to the treatment of rivers in CESM; there are significant local, regional, and remote effects. The EBM now is included as an option in CESM version 2. A future paper will compare CESM to an appropriate observational coastal climatology and explore dynamical changes introduced by rivers.

Acknowledgements

We are indebted to Rich Garvine for inspiring this research. We thank Parker MacCready for formative discussions throughout this research and thank the editor and anonymous reviewers for their many helpful comments. We also thank high-performance computing support from Yellowstone (ark:/85065/d7wd3xhc) provided by NCAR's Computational and Information Systems Laboratory, sponsored by the National Science Foundation. This work was supported by the U.S. Department of Energy, Office of Biological and Environmental Research under grant DE-SC0006814. FOB was

supported by the National Science Foundation through its sponsorship of NCAR.

Appendix

The tidal pumping of salt through the mouth upper-layer (represented as a horizontally diffusive flux in subtidal analysis) is derived in this section. Stommel and Farmer (1952) propose that the estuarine outflow into the ocean has a jet-like form during ebb tide and the inflow during flood is entrained from a semi-circular zone. Thus, much of the water passing into the mouth is not the same as the water that left the estuary during the preceding ebb. The net effect over a tidal cycle is oceanic water near the estuarine mouth is pumped into the estuary and some freshwater is ejected to the coastal ocean (Fig. A1). Tidal pumping drives a tidally-averaged salt mass (and salinity) flux and PE flux into estuary; it acts as a horizontal diffusive flux in the subtidal balances. MacCready (2004) parameterizes the horizontal diffusivity at mouth of the estuaries based on the tidal pumping concept. The EBM development also is parameterized by following this idea and the flood entrainment region is generalized to a semi-ellipse that accommodates both narrow mouths (previously considered) and wider mouths relative to the tidal excursion (Fig. A1).

The tidal pumping derivation begins with specifying the jet-like water mass lost during ebb: $M_{ebb}=\rho_{UM}WL_t(H-h)$. The water mass gained during flooding is: $M_{flood}=[\rho_{UM}(WL_t-A)+\rho_{LM}A](H-h)$, where L_t is the tidal excursion (specified below) and A is the non-overlapping area between the ebb jet and flood inflow zone. For simplicity, it is assumed that the oceanic inflow water (from the non-overlapping part of the flood inflow) has the same density as the water through the lower layer mouth. Note that the tidal exchange volume $WL_t(H-h)$ is the same for flood and ebb. The net mass change in one tidal cycle is: $\Delta M=M_{flood}-M_{ebb}=a_t(\rho_{LM}-\rho_{UM})WL_t(H-h)$, with $a_t=A/(WL_t)$. The coefficient a_t is the ratio of the non-overlapping volume (of oceanic water) to the total ebb/flood exchange volume. The tidal excursion (L_t) is defined in terms of the tidal current amplitude (u_t) of the linear sinusoidal tidal wave with tidal period T_t (Eq. (A1)); L_t is the distance water moves out from the estuary on ebb.

$$L_t=\int_0^{\frac{T_t}{2}} u_t\sin(\omega t)dt=\frac{T_t}{\pi}u_t \tag{A1}$$

The average volume flux magnitude during either flood or ebb is found by dividing the tidal exchange volume by half the tidal period (Eq. (A2)).

$$Q_{Ut}=2\frac{u_t}{\pi}W(H-h) \tag{A2}$$

Vertically and horizontally integrating the horizontal diffusion term in the continuous PE balance (Eq. 4), applying the no-diffusive-flux conditions at the head and lower-layer at the mouth, and representing the upper-layer horizontal density gradient as $a_0(\rho_{LM}-\rho_{UM})/L_t$ gives the horizontal diffusive mass flux (Eq. A3).

$$\int_{-L}^{0}\int_0^H \frac{\partial}{\partial x}\left[K_H\frac{\partial(PE)}{\partial x}\right]dzdx=\frac{1}{2}K_{HM}\frac{\rho_{LM}-\rho_{UM}}{L_t}g\left(H^2-h^2\right)$$
$$=\frac{1}{2}a_0a_t(\rho_{LM}-\rho_{UM})\frac{Q_{Ut}}{2W}g(H+h) \tag{A3}$$

The parameter a_0 is introduced because of the approximation of the horizontal density gradient at the estuary mouth. An analogous substitution is made for the horizontal diffusive flux in the PE balance (Eq. (7) and Eq. (13)). For completeness, the horizontal diffusivity is found in Eq. (A4) by assuming the horizontal diffusion at the estuary mouth is due to net mass flux from tidal pumping averaged over the entire tidal period.

$$K_{HM}=a_0a_t\frac{L_t^2}{T_t}=a_0a_t\frac{L_tu_t}{\pi} \tag{A4}$$

MacCready (2007) finds that horizontal diffusivity is overestimated by using Stommel and Farmer (1952), so he gives a reduction factor by $\varepsilon=0.1$. In the current development of the EBM, the a_0 is the corresponding free parameter. If the a_0 bigger than 1, it is reveals that the horizontal density gradient at estuary mouth is sharper than $(\rho_{LM}-\rho_{UM})/L_t$. The a_t is the tidal pumping geometric ratio for flood zone, which can vary from a semi-ellipse to a semicircle. The product of the semi-major (r_1) and semi-minor (r_2) axes of the semi-ellipse that equals the flood jet area is given by Eq. (A5).

$$r_1r_2=\frac{2WL_t}{\pi} \tag{A5}$$

The solutions for each radius are given by Eq. (A6) and Eq. (A7).

$$r_2=\begin{cases}L_t & W>\pi L_t/2\\ \sqrt{2WL_t/\pi} & W\le\pi L_t/2\end{cases} \tag{A6}$$

$$r_1=\frac{2WL_t}{\pi r_2} \tag{A7}$$

The sector angle θ in all cases is defined in equation (Eq. (A8)), where r_s (Eq. (A9)) is the radius along sector angle θ (Fig. (A1)).

$$\theta=\sin^{-1}\left(\frac{W}{2r_s}\right) \tag{A8}$$

$$r_s=\sqrt{L_t^2-\frac{W^2}{4r_2^2}\left(L_t^2-r_2^2\right)} \tag{A9}$$

For the semi-elliptical (wide-mouth) case (Fig. A1b), the a_t equation (Eq. (A10)) involves the semi-major axis r_2 (Eq. (A6)), the sector angle θ (Eq. (A8)) and the ellipse radius along the sector angle (r_s) calculated with equation (Eq. (A9)):

$$a_t=1-\frac{2F+\frac{W}{2}r_s\cdot\cos(\theta)}{WL_t}$$

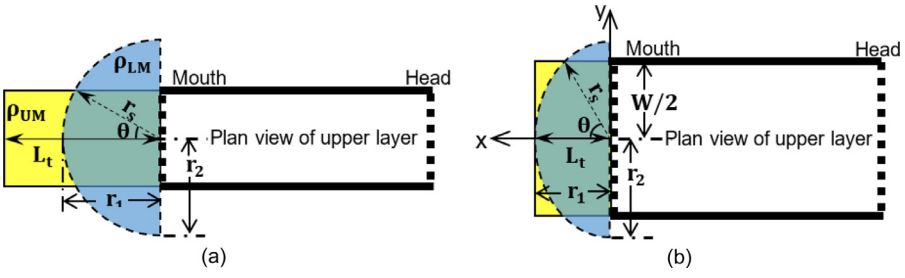

Fig. A1. Schematic representation of tidal pumping effects in EBM upper layer for estuaries with (a) a narrow mouth and/or strong tides and (b) a wide mouth and/or weak tides. The yellow shade indicates the water released during ebbs and the blue shade shows the oceanic inflow water during floods (the green shade indicates the overlap region). The ebb and flood regions have the same water volume. The parameters marked with arrows are described in the appendix. (For interpretation of the references to color in this figure legend, the reader is referred to the web version of this article.)

$$\text{with } F = \frac{L_t r_2}{2}\left\{\theta + \tan^{-1}\left[\frac{(L_t - r_2)\cdot \sin(\pi - 2\theta)}{(L_t + r_2) + (L_t - r_2)\cdot \cos(\pi - 2\theta)}\right]\right\} \tag{A10}$$

For cases where the mouth is relatively narrow and/or tides are strong (Fig. A1a), the flood zone becomes semicircular ($r_1 = r_2 = r_S$) and the surface area ratio a_t is calculated by equation (Eq. (A11)).

$$a_t = 1 - \frac{\frac{2WL_t}{\pi}\cdot\theta + \frac{W}{2}\sqrt{\frac{2WL_t}{\pi}}\cdot\cos(\theta)}{WL_t} \tag{A11}$$

If the overlap area is simplified as a rectangular, then the K_{HM} solution will be same as MacCready (2004) employed.

References

Barthem, R.B., Schwassmann, H.O., 1994. Amazon river influence on the seasonal displacement of the Salt Wedge in the Tocantins River Estuary, Brazil, 1983-1985. Museu Paraense Emilio Goeldi 10 (1), 119–130.

Bone, D., Rodriguez, C. T. & Chollett, I., 2011. Polychaeta Diversity in the Continental Shelf Off the Orinoco River Delta, Venezuela. In: O. Grillo, ed. Changing Diversity in Changing Environment. ISBN: 978-953-307-796-3, s.l.:InTech, pp. 87–97.

Burenkov, V.I., Vasil'kov, A.P., 1995. The influence of runo from land on the distribution of hydrologic characteristics of the Kara Sea. *Oceanology, English Translation* 34 (5), 591–599.

Cauwet, G., Sidorov, I., 1996. The biogeochemistry of Lena River: organic carbon and nutrients distribution. Mar. Chem. 53 (3), 211–227.

Coles, V.L., et al., 2013. The pathways and properties of the Amazon River Plume in the tropical North Atlantic Ocean. J. Geophys. Res. 118 (12), 6894–6913.

Dai, A., Trenberth, K.E., 2002. Estimates of freshwater discharge from continents: latitudinal and seasonal variations. J. Hydrometeorol. 3 (6), 660–687.

Danabasoglu, G., et al., 2012. The CCSM4 Ocean Component. J. Clim. 25 (5), 1361–1389.

Durack, P.J., 2015. Ocean salinity and the global water cycle. Oceanography 28 (1), 20–31.

Dyer, K.R., 1998. Estuaries: A Physical Introduction, 2nd Edition s.l.:John Wiley & Sons.

Egbert, G.D., Erofeeva, S.Y., 2002. Efficient inverse modeling of barotropic ocean tides. J. Atmos. Oceanic Techn. 19 (2), 183–204.

Eisma, D., Van Bennekom, J., 1978. The Zaire river and estuary and the Zaire outflow in the Atlantic Ocean. Neth. J. Sea Res. 12 (3-4), 255–272.

Emmerton, C.A., Lesack, L.F.W., Vincent, W.F., 2008. Nutrient and organic matter patterns across the Mackenzie River, estuary and shelf during the seasonal recession of sea-ice. J. Mar. Syst. 74 (3), 741–755.

Fossati, M., Piedra-Cueva, I., 2008. Numerical modelling of residual flow and salinity in the Rio de la Plata. Appl. Math. Modell. 32 (6), 1066–1086.

Garvine, R.W., McCarthy, R.K., Wong, K.-C., 1992. The axial salinity distribution in the delaware estuary and its weak response to river discharge. Estuarine Coastal Shelf Sci. 35 (2), 157–165.

Garvine, R.W., Whitney, M.M., 2006. An estuarine box model of freshwater delivery to the coastal ocean for use in climate models. J. Mar. Res. 64 (2), 173–194.

Georgiou, I.Y., Hanegan, K., 2013. Hydrodynamics and salinity modeling in the lowermost Mississippi River and Delta. Mississippi River Hydrodynamic and Delta Management Study (MRHDM) Meeting.

Geyer, R.W., 1995. Tide-induced mixing in the Amazon frontal zone. J. Geophys. Res. 100 (C2), 2341–2353.

Geyer, R.W., 2010. Estuarine salinity structure and circulation. In: Contemporary Issues in Estuarine physics, Transport and Water Quality. Cambridge University Press, New York, pp. 12–26.

Giddings, S.N., et al., 2014. Hindcasts of potential harmful algal bloom transport pathways on the Pacific Northwest coast. J. Geophys. Res. 119 (4), 2439–2461.

Godin, G., 1972. The Analysis of Tides. University of Toronto Press Toronto, Buffalo.

Griffies, S.M., et al., 2009. Coordinated ocean-ice reference experiments (COREs). Ocean Modell. 26 (1), 1–46.

Griffies, S.M., et al., 2005. Formulation of an ocean model for global climate simulations. Ocean Sci. 1 (1), 45–79.

Hansen, D.V., Rattray, M., 1966. New dimensions in estuary classification. Limnol. Oceanogr. 11 (3), 319–326.

Herzfeld, M., 2015. Methods for freshwater riverine input into regional ocean models. Ocean Modell. 90, 1–15.

Hordoir, R., Polcher, J., Brun-Cottan, J.C., Madec, G., 2008. Towards a parametrization of river discharges into ocean general circulation models: a closure through energy conservation. Climate Dyn. 31 (7-8), 891–908.

Huijts, K.M.H., Schuttelaars, H.M., de Swart, H.E., Friedrichs, C.T., 2009. Analytical study of the transverse distribution of along-channel and transverse residual flows in tidal estuaries. Cont. Shelf Res. 29 (1), 89–100.

Ianniello, J.P., 1979. Tidally induced residual currents in estuaries of variable breadth and depth. J. Phys. Oceanogr. 9 (5), 962–974.

Ianniello, J.P., 1981. Comments on tidally induced residual currents in estuaries: Dynamics and near-bottom flow characteristics. J. Phys. Oceanogr. 11 (1), 126–134.

Ingram, G.R., El-Sabh, M.I., 1990. Fronts and mesoscale features in the St. Lawrence estuary. In: Oceanography of a Large-Scale Estuarine System. Springer, New York, pp. 71–93.

IHO, IOC, BODC, 2003. Centenary Edition of the GEBCO Digital Atlas, Published On CD-ROM On Behalf of the Intergovernmental Oceanographic Commission and the International Hydrographic Organization as Part of the General Bathymetric Chart of the Oceans. British Oceanographic Data Centre, Liverpool, U.K.

Jana, S., Gangopadhyay, A., Chakraborty, A., 2015. Impact of seasonal river input on the Bay of Bengal simulation. Cont. Shelf Res. 104, 45–62.

Kravtsova, V.I., Mikhailov, V.N., Kidyaeva, V.M., 2009. Hydrological regime, morphological features and natural territorial complexes of the Irrawaddy River Delta (Myanmar). Water Res. 36 (3), 243–260.

Lagarias, J.C., Reeds, J.A., Wright, M.H., Wright, P.E., 1998. Convergence properties of the Nelder–Mead simplex method in low dimensions. SIAM J. Optim. 9 (1), 112–147.

Large, W.G., Yeager, S.G., 2009. The global climatology of an interannually varying air–sea flux data set. Clim. Dyn. 33 (2-3), 341–364.

MacCready, P., 1999. Estuarine adjustment to changes in river flow and tidal mixing. J. Phys. Oceanogr. 29 (4), 708–726.

MacCready, P., 2004. Toward a unified theory of tidally-averaged estuarine salinity structure. Estuaries 27 (4), 561–570.

MacCready, P., 2007. Estuarine adjustment. J.Phys. Oceanogr. 37 (8), 2133–2145.

MacCready, P., 2011. Calculating estuarine Exchange flow using isohaline coordinates. J. Phys. Oceanogr. 41 (6), 1116–1124.

MacCready, P., Geyer, R.W., 2010. Advances in estuarine physics. Ann. Rev. of Mar. Sci. 2, 35–58.

Nguyen, A.D., Savenije, H.H.G., Pham, D.N., Tang, D.T., 2008. Using salt intrusion measurements to determine the freshwater discharge distribution over the branches of a multi-channel estuary: the Mekong Delta case. Estuarine, Coastal Shelf Sci. 77 (3), 433–445.

Rahaman, H., et al., 2014. Development of a regional model for the North Indian ocean. Ocean Modell. 75, 1–19.

Rao, Y.R., 2005. Modelling of circulation and salinity in a tidal estuary. J. Coastal Res. (SI 42) 363–369.

Rice, A.E., Whitney, M.M., Garvine, R.W., Huq, P., 2008. Energetics in Delaware Bay: comparison of two box models with observations. J. Marine Res. 66 (6), 873–898.

Saucier, F.J., Roy, F., Gilbert, D., 2003. Modeling the formation and circulation processes of water masses and sea ice in the Gulf of St. Lawrence, Canada.. J. Geophys. Res. Oceans 108(C8).

Shevchenko, O.G., et al., 2013. Phytoplankton of the Amur River Estuary (Sea of Okhotsk) during the summer periods of 2005–2007. Russ. J. Mar. Biol. 39 (2), 92–106.

Simpson, J.H., Brown, J., Matthews, J., Allen, G., 1990. Tidal straining, density currents, and stirring in the control of estuarine stratification. Estuaries 13 (2), 125–132.

Stommel, H.M., Former, H.G., 1952. On the Nature of Estuarine circulation: Part I (Chapters 3 and 4). s.l.:Woods Hole Oceanographic Institution.

Tseng, Y.-H., Bryan, F.O., Whitney, M.M., 2016. Impacts of the representation of riverine freshwater input in the community earth system model. Ocean Modell. 105, 71–86.

Vinayachandran, P.N., Murty, V.S.N., Babu, V.R., 2002. Observations of barrier layer formation in the Bay of Bengal during summer monsoon. J. Geophys. Res. 107 (C12) SRF-19.

Yin, J., Stouffer, R.J., Spelman, M.J., Griffies, S.M., 2010. Evaluating the uncertainty induced by the virtual salt flux assumption in climate simulations and future projections. J. Climate 23 (1), 80–96.

Zhang, E., et al., 2011. Analytical solution for salt intrusion in the Yangtze Estuary, China. Estuarine, Coastal Shelf Sci. 91 (4), 492–501.

Zu, T., Gan, J., 2015. A numerical study of coupled estuary–shelf circulation around the Pearl River Estuary during summer: Responses to variable winds, tides and river discharge. Deep Sea Res. 117, 53–64.

Zweng, M.M., et al., 2013. World Ocean Atlas 2013, Volume 2: Salinity. In: Levitus, S., Technical, M.A. (Eds.). In: NOAA Atlas NESDIS, 74, p. 39. s.l.:s.n..